https://doi.org/10.17221/39/2025-SWR

Rainfall pattern impact on runoff and sediment of the sloping cropland in Northeast China

Xu Fan[1], Wei Hu[2], Zhongzheng Ren[1], Yuan Chen[2], Qingsong Shen[2], Xingyi Zhang[1,2]**

[1]*School of Resources and Environment, Northeast Agricultural University, Harbin, P.R. China*
[2]*State Key Laboratory of Black Soils Conservation and Utilization, Northeast Institute of Geography and Agroecology, Chinese Academy of Sciences, Harbin, P.R. China*

**Corresponding author: huwei@iga.ac.cn; zhangxy@iga.ac.cn*

Citation: Fan X., Hu W., Ren Z.Z., Chen Y., Shen Q.S., Zhang X.Y. (2026): Rainfall pattern impact on runoff and sediment of the sloping cropland in Northeast China. Soil & Water Res., 21: 9–19.

Abstract: Rainfall is a major contributor to water erosion of sloping cropland in Northeast China. Identifying how rainfall and slope gradient (*S*) influence runoff depth (*RD*) and sediment yield (*SY*) is crucial for preventing water erosion. Field measurements from runoff plots were collected from 2023 to 2024, and *K*-means clustering was applied to clarify the rainfall patterns. Response of *RD* and *SY* to the rainfall pattern and *S* were analysed. Key factors impacting *RD* and *SY* were explored. The results showed that three rainfall patterns were identified for 34 erosive rainfall events: A (41.2%, medium duration, medium rainfall intensity, and medium rainfall amount (*RA*)). B (50.0%, short duration, high rainfall intensity, and low *RA*) and C (5.4%, long duration, low rainfall intensity, high *RA*). Furthermore, the cumulative *RD* and *SY* increased with *S* for the same rainfall pattern. The cumulative *RD* and *SY* responded similarly to rainfall patterns for the same *S*. The contribution of the rainfall pattern to the cumulative *RD* and *SY* decreased in the order of C, A, and B. In addition, rainfall duration (*D*) and maximum 30-minute rainfall intensity were the key factors affecting *RD* and *SY* for rainfall pattern A, respectively. Rainfall erosivity (*R*) was the key factor affecting *RD* and *SY* for rainfall pattern B and C. *R* and *RD* were the dominant factors influencing the *RD* and *SY* for all rainfall events, respectively.

Keywords: black soil region; natural rainfall; rainfall erosivity; soil and water loss

Soil erosion is a global environmental problem (Wei et al. 2023; Juliev et al. 2024), resulting in land degradation (Yao et al. 2016). Rainfall is the primary cause of water erosion (Tao et al. 2017; Jia et al. 2022; Yang et al. 2022; Wang et al. 2024). The rainfall intensity changes during the natural rainfall process (Frauenfeld & Truman 2004; Peng & Wang 2012; Wu et al. 2017), leading to various rainfall patterns (Wei et al. 2007; Wen et al. 2012) with different rainfall amounts, intensities, durations, and erosivities (Parsons & Stone 2006). Researchers have investigated the correlation between rainfall patterns and the amount of soil and water loss using rainfall simulations. For example, Flanagan et al. (1988) found that the peak runoff amount of dry soils was 4 to 20 times larger during peak rainfall intensity in the late stage than for uniform rainfall intensity and peak rainfall intensity in other stages. Parsons and Stone (2006)

Supported by the National Key Research and Development Program of China, Project No. 2024YFD1501105, the Young Scientist Group Project of Northeast Institute of Geography and Agroecology, Chinese Academy of Sciences, Project No. 2023QNXZ03, and the Heilongjiang Key Research and Development Program (Innovation Base) Project (JD24A012).

https://doi.org/10.17221/39/2025-SWR

noted that the rainfall pattern did not significantly impact the runoff amount but significantly affected the sediment yield (*SY*). Furthermore, field data from runoff plots have been used to analyse the correlation between rainfall patterns and water erosion. Sobol et al. (2017) and Nishigaki et al. (2017) reported that high rainfall intensity with long duration or high rainfall amount (*RA*) were the dominant factors contributing to cropland soil erosion in the Nanshun Ural region and Tanzania. Pena-Angulo et al. (2020) observed that rainfall pattern with short duration, medium intensity, and high *RA* had the largest effect on soil erosion in the coastal region of Spain. Qin et al. (2015) stated that low *RA* with high intensity and short duration contributed the most to water erosion in the red loam region of China. Therefore, the rainfall pattern influencing water erosion differs significantly in different regions.

In addition to rainfall, the topography also affects soil erosion (Neves dos Santos et al. 2017; Londero et al. 2021). The slope gradient (*S*) substantially influences soil and water loss by impacting soil infiltration (Nord & Esteves 2010; Shen et al. 2021) and overland runoff velocity (Chaplot & Le Bissonnais 2003; Meng et al. 2021). Numerous studies have shown that the impact of *S* on soil erosion is highly complex. Hofbauer et al. (2023) noted that the runoff and sediment amounts increased with an increase in *S* in the Czech Republic. The reason is the higher runoff velocity on steeper slopes, resulting in more soil particle movement. Defersha et al. (2011) and Balacco (2013) observed that the runoff depth (*RD*) and *SY* firstly increased, then decreased with an increase in *S* in the Ethiopian Plateau and sandy loam region in southern Italy, respectively; a critical *S* threshold was identified. Wu et al. (2018) and Balacco (2013) also found the critical *S* threshold in the loess plateau and southern Italy, respectively; the runoff did not accumulate after *S* exceeded the critical *S*, resulting in a decrease in soil erosion. Therefore, regional differences exist in the quantitative relationship between *S* and the soil erosion rate.

Northeast China is a critical food production area (Bai et al. 2024). However, regional soil erosion has become a serious problem due to extensive development in recent years (Liu et al. 2021; Yan et al. 2023). The annual decrease rate of the black soil layer is approximately 2 to 3 mm (Dai et al. 2022). Nearly 80% of the precipitation in this area falls in summer (Zhan et al. 1998; Zhang et al. 2020a; Dai et al. 2022). Long, gentle slopes are common in this region (Wang et al. 2022). The dominant farming practice is longitudinal ridge tillage, which causes runoff accumulation and soil erosion (Zhang et al. 2020b; Ding et al. 2024). Therefore, the unique rainfall pattern and topographic characteristics are the main factors influencing water erosion in Northeast China. However, most studies on the effect of rainfall patterns on water erosion of sloping cropland have used rainfall simulations (Wen et al. 2012; Zheng et al. 2016), which do not provide information on water erosion under natural rainfall conditions. In addition, the gentle slopes in this region are unique in China. Thus, more research is required to understand the effects of rainfall patterns on cropland erosion in this area. Therefore, this study is based on data from two consecutive years of monitoring runoff plots. The objectives are to (1) clarify the rainfall pattern, (2) analyse the *RD* and *SY* for different rainfall patterns and *S*, and (3) determine the key factors affecting the *RD* and *SY* for different rainfall patterns.

MATERIAL AND METHODS

Study area. The study was conducted at the Hailun soil and water conservation monitoring station, Chinese Academy of Sciences, located in the Guangrong small watershed (47°21'16.95''N, 126°49'56.43''E), Heilongjiang Province, Northeast China. This region has a monsoon climate with cold-dry winters and hot-rainy summers. The annual *RA* ranges from 500 to 600 mm, and > 50% of the rainfall occurs from June to August. The annual air temperature and annual effective cumulative temperature (≥ 10 °C) are 1.5 °C and 2 450 °C, respectively. The area is located in the black soil zone of the Songnen Plain. The topography is hilly, the *S* is 3° to 8°, and the average elevation is 210 m. The black soil has a thickness of approximately 30 cm. The soil organic matter content is 42.1 g/kg, and the clay, sand, and silt contents are 37.6%, 31.6%, and 30.8%, respectively. Corn and soybean are grown in rotation.

Experimental design and measurements. Six runoff plots with an area of 90 m^2 (20 × 4.5 m) were established in a cropland area. Three plots had slopes of 5° and three had slopes of 7°. Longitudinal ridge tillage was used (20 cm ridge with 65 cm furrow), and manual weeding was performed twice during the seedling stage. The ridges were re-established twice during the growing season using inter-tillage, and after the harvest in the fall using rotary tillage. The runoff plots were planted in a maize-soybean rotation system, i.e., maize in 2023 and soybean in 2024. The rainfall conditions were monitored in the rainy

https://doi.org/10.17221/39/2025-SWR

season of 2023 to 2024 (June to September, 556.1 mm on average). A tipping bucket rain gauge was used to record the rainfall process. The rainfall parameters were calculated using RainRecord 1.06 software, including *RA*, rainfall duration (*D*), average rainfall intensity (*I*), maximum 30 min rainfall intensity (I_{30}), and rainfall erosivity (*R*). Soil and water loss were measured using a runoff and sediment monitoring device (XYZ-III, Northeast Institute of Geography and Agroecology, Chinese Academy of Sciences, Harbin, China) (Sun et al. 2014). A HOBO data logger was used to record runoff. The runoff sample was dried and weighed at 105 °C, and the *SY* and sediment concentration were calculated. New runoff bottles were used before the next rainfall. The vegetation coverage (*VC*) was estimated using images acquired by an unmanned aerial vehicle (UAV) every 15 days from May 15 to September 30.

Data analysis. The *R* was calculated as follows:

$$R = EI_{30} \quad (1)$$

$$E = \sum^{n}_{r=1}(e_r \times p_r) \quad (2)$$

$$e_r = 0.29[1 - 0.72\exp(-0.082i_r)] \quad (3)$$

where:

E – the kinetic energy of a rainfall event (MJ/ha);
I_{30} – the maximum 30-min rainfall intensity (mm/h);
e_r – the per unit rainfall energy (MJ/(ha mm));
p_r – the rainfall amount during period r (mm);
i_r – the rainfall intensity during period r (mm/h);
r – the rainfall period divided into 1, 2, 3, ..., n periods according to the rainfall intensity.

SPSS 21.0 statistical software was used to determine the descriptive statistics and the distribution of the rainfall parameters; *K*-means clustering was applied to analyse the rainfall pattern. Significant differences in the *VC* were examined during the observation period, and the difference in the *RD* and *SY* were also examined for various rainfall patterns or slope gradients. Correlation analysis between *RD* and *SY* with different variables was performed. The highest correlations between *RD* and *SY* with different variables were determined using stepwise regression analysis.

Considering the existence of multiple linear correlations between the influencing variables, the relationship between *RD* and *SY* and the influencing variables was analysed using the partial least squares regression, which was performed using SIMCA-P 11.5 software. We used two parameters to assess model fit. R^2Y represents the portion of the model fit that accounts for the variation of the *Y* variable (dependent variable). Q^2 represents the portion of the model assessed by cross-validation, it predicts the variation of the *Y* variable. Values of R^2Y and Q^2 close to 1.0 indicate a high model. The variable importance (*VIP*) values were used to determine the variable importance. A variable with a *VIP* > 1 has a larger contribution to the *Y* variable.

The plots were drawn using OriginPro 2024b software.

RESULTS

Characteristics of erosive rainfall events. Thirty-four erosive rainfall events were recorded during the observation period, accounting for 30.4% of the total rainfall events (112); non-erosive rainfall events occurred before 25 erosive rainfall events (Figure 1). The *RA* ranged from 4.0 to 180.6 mm, *D* ranged from 20 to 3 175 min (Figure 2), *I* ranged from 0.7 to 24.0 mm/h, I_{30} ranged from 3.6 to 50.8 mm/h, and *R* ranged from 2.2 to 2 006.9 (MJ mm)/(ha h). According to 3 rainfall parameters (*RA*, *D*, and I_{30}), three rainfall patterns were identified for 34 erosive rainfall events (A, B, and C; Table 1, $P < 0.05$). Rainfall pattern A (41.2%) had medium *D* (560–1490 min), medium *I* (0.7–3.9 mm/h), and medium *RA* (10.6 to 69.4 mm). Rainfall pattern B (50.0%) exhibited short *D* (20–500 min), high *I* (1.0–24.0 mm/h), and low *RA* (4.0–38.6 mm). Rainfall pattern C (5.4%) was characterised by long *D* (2685–3175 min), low *I* (0.8–4.0 mm/h), and high *RA* (40.6–180.6 mm). The *I* of rainfall pattern A and C was similar; it was 29% of the *I* of rainfall pattern B. Rainfall patterns A, B, and C predominantly occurred from August to September, June to July, and August, respectively. Their frequencies accounted for 64.3%, 58.8%, and 66.7%, and their *RA* accounted for 79.1%, 71.9%, and 75.8%, correspondingly. The *VC* ranged from 3.0% to 96.8% and 13.2% to 95.5% for maize and soybean, respectively; it increased rapidly, increased slowly, kept a steady state, and decreased slowly during the monitoring period (Figure S1 in Electronic Supplementary Material (ESM), $P < 0.05$).

Runoff and sediment. No significant difference was found in the average *RD* and *SY* between different *S*

https://doi.org/10.17221/39/2025-SWR

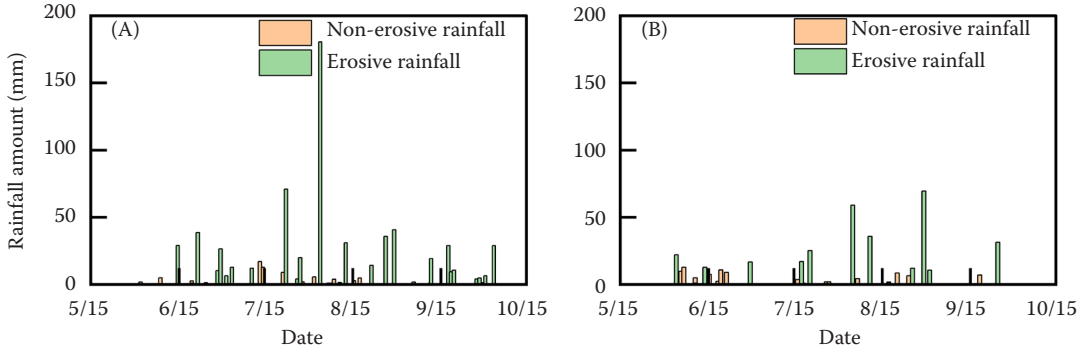

Figure 1. Non-erosive and erosive rainfall events in 2023 (A) and 2024 (B)

(Figure 3). A significant difference in the average *RD* and *SY* was observed among different rainfall patterns (Figure 4, P < 0.05). The average *RD* and *SY* for rainfall pattern C was 9.8 and 24.3, 22.7 and 13.4 times higher than for rainfall pattern A and B, respectively. Furthermore, a significant difference occurred in the average *SY* between different *S* for rainfall pattern A (Figure 5, $P < 0.05$). As the *S* increased from 5° to 7°, the *SY* increased by 2.9 times. Significant difference in the average *RD* and *SY* was found among different rainfall patterns at the same *S* (Figure 5, $P < 0.05$). For an *S* of 5°, the average *RD* and *SY* were 9.1 and 44.0, and 14.4 and 16.5 times higher for rainfall pattern C than for rainfall pattern A and B, respectively. For an *S*

Table 1. Descriptive statistics of different rainfall patterns

Rainfall pattern	Sample size	Parameter	*RA* (mm)	*D* (min)	*I* (mm/h)	I_{30} (mm/h)	*R* (MJ mm)/(ha h)
		mean	30.6	856	2.2	17.2	148.5
		min	10.6	560	0.7	3.6	4.8
		P25	16.2	620	1.3	7.6	29.8
A	14	median	28.9	795	2.2	10.4	49.2
		P75	35.8	1 031	3.0	26.6	177.3
		max	69.4	1 490	3.9	40.4	618.4
		SD	16.6	270	1.0	12.3	201.6
		mean	13.8	185	7.3	20.3	95.3
		min	4.0	20	1.0	3.6	2.2
		P25	6.4	58	2.5	8.4	10.1
B	17	median	12.0	205	6.0	19.6	49.4
		P75	19.6	275	10.4	27.2	140.2
		max	38.6	500	24.0	50.8	465.4
		SD	9.2	135	5.9	13.6	120.7
		mean	97.3	2 853	2.1	25.1	772.9
		min	40.6	2 685	0.8	9.6	57.4
		P25	40.6	2 685	0.8	9.6	57.4
C	3	median	70.8	2 700	1.6	20.0	254.5
		P75	–	–	–	–	–
		max	180.6	3 175	4.0	45.6	2 007.0
		SD	73.7	279	1.7	18.5	1 073.2

RA – rainfall amount; *D* – rainfall duration; *I* – average rainfall intensity; I_{30} – maximum 30 min rainfall intensity; *R* – rainfall erosivity; P25 – lower quartile value; P75 – upper quartile value; SD – standard deviation

https://doi.org/10.17221/39/2025-SWR

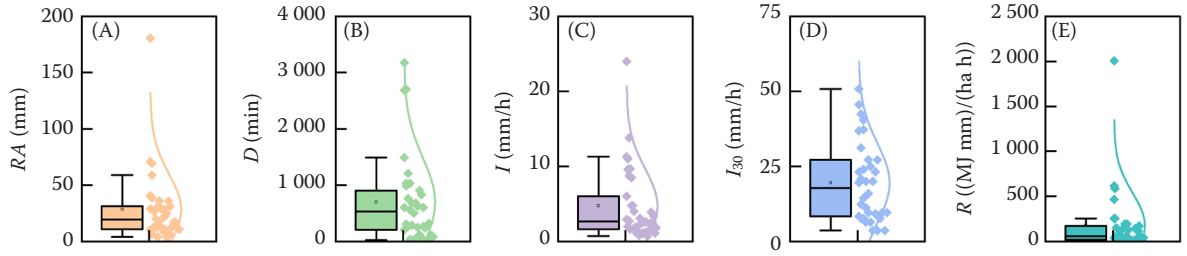

Figure 2. Rainfall parameters of erosive rainfall events: (A) *RA*, (B) *D*, (C) *I*, (D) I_{30}, (E) *R*
RA – rainfall amount; *D* – rainfall duration; *I* – average rainfall intensity; I_{30} – maximum 30 min rainfall intensity; *R* – rainfall erosivity

of 7°, the average *RD* and *SY* were 8.4 and 17.4, and 22.7 and 13.6 times higher for rainfall pattern C than for rainfall pattern A and B, respectively.

For the same *S*, the cumulative *RD* was similar for different rainfall patterns (Figure 6). The contribution of the rainfall pattern to the cumulative *RD* de-

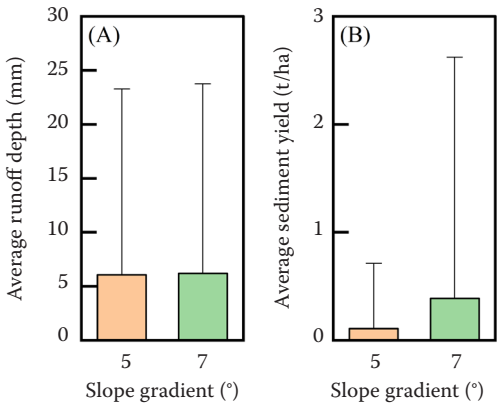

Figure 3. Average runoff depth (A) and sediment yield (B) for different slope gradients

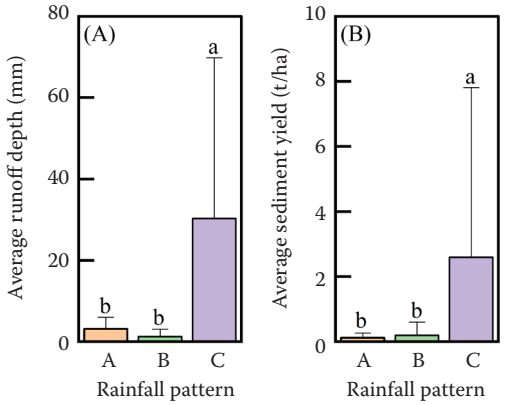

Figure 4. Average runoff depth (A) and sediment yield (B) for different rainfall patterns
Lowercase letters indicate that the value is significantly different for different rainfall patterns

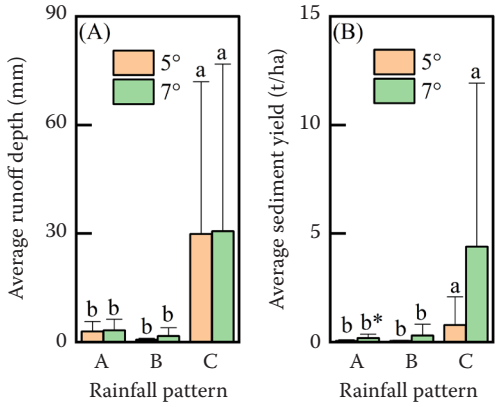

Figure 5. Interaction effect of rainfall pattern and slope gradient on average runoff depth (A) and sediment yield (B)
*Indicates that the value is significantly different for different slope gradients, $P < 0.05$; lowercase letters indicate that the value is significantly different at different rainfall patterns

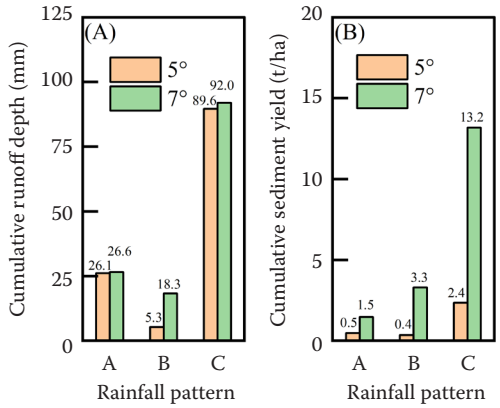

Figure 6. Interaction effect of rainfall pattern and slope gradient on cumulative runoff depth (A) and sediment yield (B)

https://doi.org/10.17221/39/2025-SWR

Table 2. Correlation coefficients between influencing factors and the runoff depth (*RD*) and sediment yield (*SY*) for different slope gradients (*S*)

Indicators	*S* (°)	*RA*	*D*	*I*	I_{30}	*R*	*VC*
RD	5	0.917**	0.538*	–0.072	0.36	0.929**	0.361
	7	0.899**	0.526*	–0.077	0.440*	0.944**	0.242
SY	5	0.899**	0.448*	–0.033	0.432	0.945**	0.272
	7	0.863**	0.458*	–0.047	0.450*	0.927**	0.196

RA – rainfall amount; *D* – rainfall duration; *I* – average rainfall intensity; I_{30} – maximum 30 min rainfall intensity; *R* – rainfall erosivity; *VC* – vegetation coverage; *, **P < 0.05, 0.01

creased in the order of C (67.2% to 74.0%), A (19.4% to 21.6%), and B (4.4% to 13.4%). For the same *S*, the cumulative *SY* differed for different rainfall patterns (Figure 6). For an *S* of 5°, the contribution of the rainfall pattern to cumulative *SY* decreased in the order of C (73.8%), A (14.8%), and B (11.4%). For an *S* of 7°, the contribution of the rainfall patterns to the cumulative *SY* decreased in the order of C (73.4%), B (18.4%), and A (8.2%). Furthermore, for the same rainfall pattern, the cumulative *RD* and *SY* were the same for different *S*. As the *S* increased, the cumulative *RD* and *SY* increased by 1.9% to 245.6%, and 2.1 to 8.1 times, respectively.

Correlation between influencing factors and the runoff depth and sediment yield. The correlation between the influencing factors and the *RD* and *SY* was similar for different *S* (Table 2). The *RD* and *SY* were significantly positively correlated with *R*, *RA*, and *D* for an *S* of 5° and with *R*, *RA*, *D*, and I_{30} for an *S* of 7°.

The correlation between the influencing factors and the *RD* and *SY* differed for different rainfall patterns. The *RD* was significantly correlated with the *RA*, *D*, I_{30}, and *R* for rainfall pattern A, B, and all rainfall patterns and with the *RA*, *I*, I_{30}, and *R* for rainfall pattern C. The *SY* was significantly correlated with the *I*, I_{30}, *R*, and *S* for rainfall pattern A, with the I_{30} and *R* for rainfall pattern B, and with the *RA*, *D*, I_{30}, and *R* for all rainfall pattern (Table 3).

Key factors influencing runoff and sediment. Partial least squares regression was used to analyse the correlation between the influencing factors and the *RD* and *SY*. The *RD* and *SY* were the dependent variables, and the *S*, *P*, *D*, *I*, I_{30}, *R*, *VC*, and *RD* were the independent variables (Table 4).

For the *RD*, at rainfall pattern A, the regression equation explained 47.1% of the variation in *RD* (R^2Y) and had 17.8% predictive ability (Q^2). Four *VIP* values were greater than 1 (Figure 7), and the contribution of the variables to the *RD* decreased in the order of *D*, *RA*, *R*, and I_{30}. The *D* was the maximum contributor (1.30). The *RD* increased with increases in *D*, *RA*, *R* and I_{30}. For rainfall pattern B, the regression equation explained 64.5% of the variation in *RD* and had 48.0% predictive ability. Four *VIP* values were greater than 1, the contribution of the variables to the *RD*

Table 3. Correlation coefficients between influencing factors and the runoff depth (*RD*) and sediment yield (*SY*) for different rainfall patterns

Indicators	Rainfall pattern	*RA*	*D*	*I*	I_{30}	*R*	*VC*	*S*
RD	A	0.725**	0.577*	0.424	0.554*	0.641**	0.264	0.17
	B	0.506*	0.466*	–0.161	0.495*	0.533*	–0.398	0.312
	C	0.963**	–0.422	0.953**	0.940**	0.987**	0.536	0.011
	all	0.907**	0.529**	–0.074	0.402**	0.936**	0.299	0.012
SY	A	0.419	–0.008	0.478*	0.711**	0.545*	0.056	0.503*
	B	0.419	0.383	–0.127	0.529*	0.519*	–0.262	0.298
	C	0.740	–0.36	0.734	0.726	0.753	0.367	0.378
	all	0.707**	0.357*	–0.028	0.370*	0.756**	0.183	0.167

RA – rainfall amount; *D* – rainfall duration; *I* – average rainfall intensity; I_{30} – maximum 30 min rainfall intensity; *R* – rainfall erosivity; *VC* – vegetation coverage; *S* – slope gradient; *, **P < 0.05, 0.01

https://doi.org/10.17221/39/2025-SWR

Table 4. Regression equation of the relationship between the influencing factors and the runoff depth (*RD*) and sediment yield (*SY*) for different rainfall patterns

Rainfall pattern	Dependent variable	Regression equation	R^2Y	Q^2
A	*RD*	$RD_1 = 1.039 + 0.195RA + 0.344D + 0.045I + 0.108I_{30} + 0.105R + 0.068VC + 0028S$	0.471	0.178
	SY	$SY_1 = 0.707 - 0.080RA - 0.238D + 0.116I + 0.360I_{30} + 0.055R - 0.133VC + + 0.268RD_1 + 0.417S$	0.605	0.282
B	*RD*	$RD_2 = 0.697 + 0.188RA + 0.169D - 0.052I + 0.206I_{30} + 0.215R - 0.144VC + 0.112S$	0.480	0.103
	SY	$SY_2 = 0.301 - 0.009RA + 0.013D + 0.031I + 0.004I_{30} - 0.006R + 0.021VC + + 0.483RD_2 + 0.009S$	0.969	0.732
C	*RD*	$RD_3 = 0.766 + 0.225RA + 0.012D - 0.217I + 0.208I_{30} + 0.247R - 0.263VC + 0.008S$	0.998	0.990
	SY	$SY_3 = 1.133 - 0.161RA + 0.272D - 0.022I + 0.068I_{30} - 0.749R - 0.097VC + + 3.903RD_3 + 0.568S$	0.979	0.910
All	*RD*	$RD_T = 0.353 - 0.597RA + 0.225D + 0.038I - 0.358I_{30} + 1.647R - 0.067VC + 0.013S$	0.954	0.674
	SY	$SY_T = 0.244 + 0.188RA - 0.030D + 0.043I + 0.044I_{30} + 0.266R - 0.142VC + + 0.391RD + 0.198S$	0.714	0.143

RD_1 – *RD* at rainfall pattern A; RD_2 – *RD* at rainfall pattern B; RD_3 – *RD* at rainfall pattern C; RD_T – *RD* at all rainfall patterns; SY_1 – *SY* at rainfall pattern A; SY_2 – *SY* at rainfall pattern B; SY_3 – *SY* at rainfall pattern C; SY_T – *SY* at all rainfall patterns; *RA* – rainfall amount; *D* – rainfall duration; *I* – average rainfall intensity; I_{30} – maximum 30 min rainfall intensity; *R* – rainfall erosivity; *VC* – vegetation coverage; *S* – slope gradient

decreased in the order of *R*, I_{30}, *RA*, and *D*. *R* was the maximum contributor (1.31). The *RD* increased with increases in *R*, I_{30}, *RA*, and *D*. For rainfall pattern C, the regression equation explained 99.8% of the variation in *RD* and had 99.0% predictive ability. Four *VIP* values were greater than 1; the contribution of the variables to the *RD* decreased in the order of *R*, *RA*, *I*, and I_{30}. The *R* was the maximum contributor (1.25). The *RD* increased with increases in *R*, *RA*, *I*, and I_{30}. For all rainfall patterns, the regression equation explained 60.1% of the variation in the *RD* and had 34.5% predictive ability. Two *VIP* values were greater than 1. The contribution of the variables to the *RD* decreased in the order of *R* and *RA*. The *R* was the maximum contributor (1.55). The *RD* increased with increases in *R* and *RA*.

For the *SY*, at rainfall pattern A, the regression equation explained 60.5% of the variation in the *SY* and had 28.2% predictive ability. Three *VIP* values were greater than 1 (Figure 8). The contribution of the variables to the *SY* decreased in the order of I_{30}, *S*, and *RA*. The I_{30} was the maximum contributor (1.27). The *SY* increased with increases in I_{30}, *S*, and *RA*. For rainfall pattern B, the regression equation explained 96.9% of the variation in the *SY* and had 73.2% predictive ability. Four *VIP* values were greater than 1. The contribution of the variables to the *SY* decreased in the order of *R*, *D*, *VC*, and *RD*. The *R* was the maximum contributor (1.45). The *SY* increased with increases in *R*, *D*, *VC*, and *RD*. For rainfall pattern C, the regression equation explained 97.9% of the variation in the *SY* and had 91.0% predictive ability. Three *VIP* values were greater than 1. The contribution of the variables to the *SY* decreased in the order of *R*, *RD*, and *S*. *R* was the maximum contributor (1.45). The *SY* increased with increases in *R*, *RD*, and *S*. For all rainfall patterns, the regression equation explained 71.4% of the variation in the *SY* and had 14.3% predictive ability. Three *VIP* values were greater than 1. The contribution of the variables to the SY decreased in the order of *RD*, *R*, and *RA*. The *RD* was the maximum contributor (1.55). The *SY* increased with increases in *RD*, *R*, and *RA*.

DISCUSSION

Rainfall pattern. Rainfall is the major contributor to water erosion (Yao et al. 2016; Pena-Angulo et al. 2020; Wei et al. 2023; Juliev et al. 2024). Differences in rainfall parameters (*RA*, *D*, *I*, I_{30}, *R*, etc.) result in different rainfall patterns (Parsons & Stone 2006; Peng & Wang 2012; Tao et al. 2017) and water erosion intensities. In this study, rainfall pattern B (short *D*, high *I*, and low *RA*) was the rainfall pattern with the highest frequency; its contribution to the cumulative *SY* was moderate. This result was in agreement with

https://doi.org/10.17221/39/2025-SWR

that of Zhan et al. (1998) and Dai et al. (2022) in this region. The possible reason was that high *I* resulted in high kinetic energy, breaking down soil aggregates; short *D* accelerates the occurrence of surface runoff, the shear force of runoff and sediment transport capacity strengthened; the low *RA* limited the total amounts of *SY* (Sobol et al. 2017). Furthermore, rainfall pattern C (long *D*, low *I*, and high *RA*) was the extreme erosive rainfall event, and contributed the most to the cumulative *SY*. This rainfall event had the largest daily *RA* (97.5 to 247.5 mm) in the 1961 to 2018 period in this region (Zhang et al. 2020a). The rainfall event on 3rd August 2023 contributed 98.1% of the total *SY* in rainfall pattern C and 72.2% of the total *SY* in the entire observation period. This rainfall pattern occurred 4 times from 2013 to 2024; thus, it should not be ignored and should be investigated to prevent soil erosion. The soil erosion of this rainfall pattern have been caused by long-time soil saturation, which decreased the soil erosion resistance

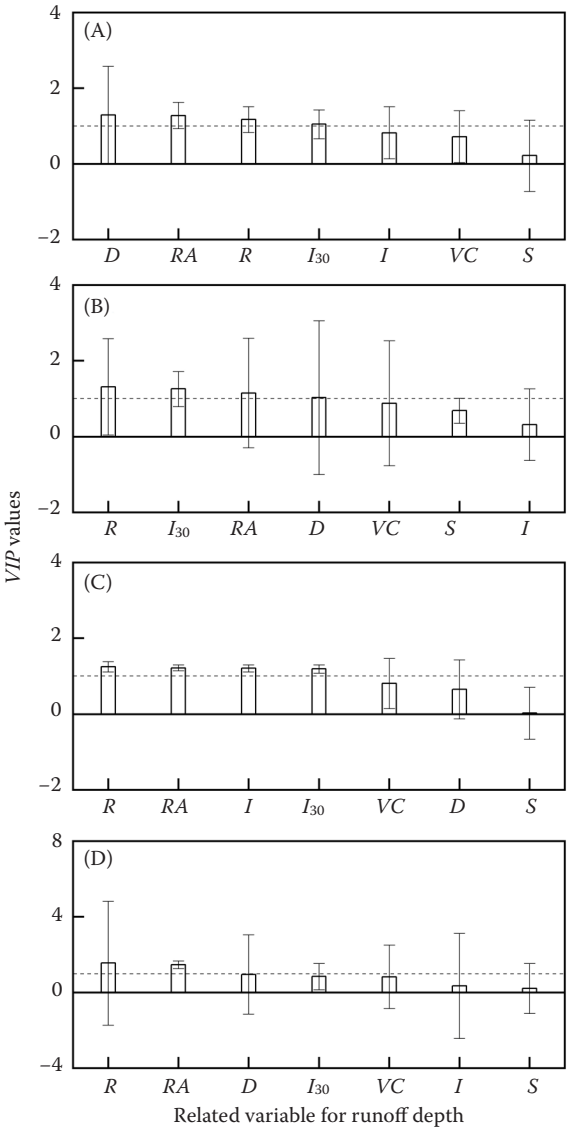

Figure 7. Variable importance (*VIP*) values for variables affecting runoff depth: A (A), B (B), C (C), and all rainfall patterns (D)
RA – rainfall amount; *D* – rainfall duration; *I* – average rainfall intensity; I_{30} – maximum 30 min rainfall intensity; *R* – rainfall erosivity; *VC* – vegetation coverage; *S* – slope gradient

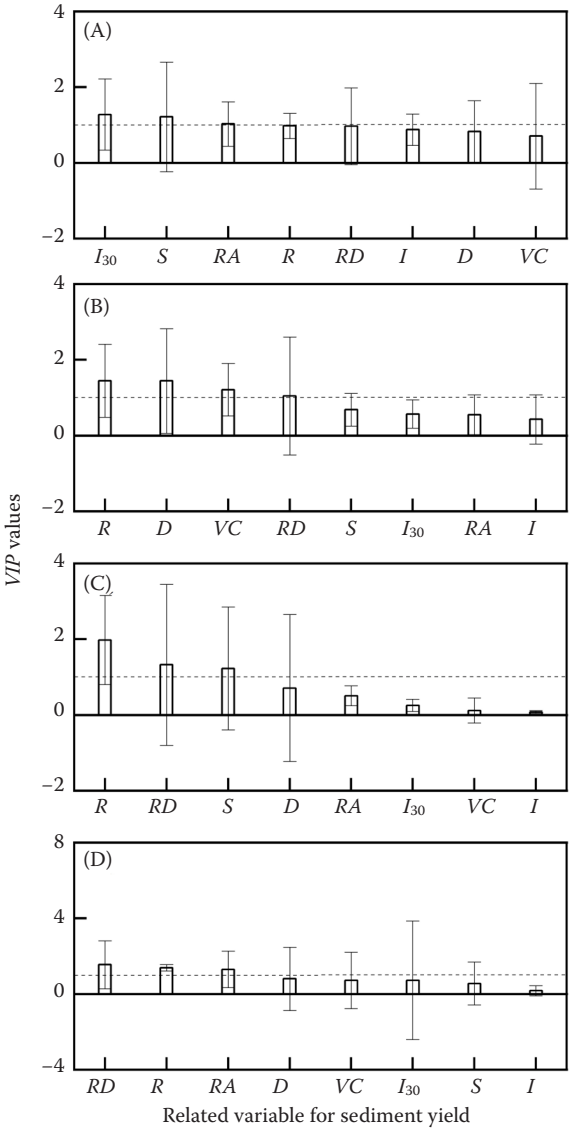

Figure 8. Variable importance (*VIP*) values for variables affecting sediment yield: A (A), B (B), C (C), and all rainfall patterns (D)
RD – runoff depth; *RA* – rainfall amount; *D* – rainfall duration; *I* – average rainfall intensity; I_{30} – maximum 30 min rainfall intensity; *R* – rainfall erosivity; *VC* – vegetation coverage; *S* – slope gradient

https://doi.org/10.17221/39/2025-SWR

(Meng et al. 2021); the runoff lasted for a long time, transporting soil particles downslope; after the soil became wet in the early stage, the sediment transport capacity of the runoff increased significantly in the later stage, contributing the most to the cumulative *SY* (Nishigaki et al. 2017). In addition, rainfall pattern A (medium *D*, *I*, and *RA*) had a medium frequency and contributed the least to the cumulative *SY*. This finding agreed with that of Ding et al. (2024) in this region, rainfall with medium *I* has limited raindrop kinetic energy, the effect of the raindrop impact on the soil surface is relative weaker, medium *RA* and *D* resulted in moderate runoff volume and sediment transport capacity (Wu et al. 2017), resulting in surface crusting (Chaplot & Le Bissonnais 2003) and stable soil infiltration rate; thus, little water erosion occurred (Yang et al. 2022). However, Yan et al. (2023) noted that moderate *D*, high *RA*, and high *I* caused the most water erosion in Northeast China. This difference could be attributed to different plot sizes, which would change the sediment transport. Other studies also reported different effects of the dominant rainfall patterns on soil erosion, which can be attributed to regional variability in climate, soil properties, and topographic factors (Wei et al. 2007; Peng & Wang 2012; Qin et al. 2015; Neves dos Santos et al. 2017).

Key factors. The *R* and *RA* were the dominant factors affecting the *RD* for all rainfall patterns. The *R* contributed the most to the *RD* because an increase in *R* increases raindrop impact energy (Zhang et al. 2020b) and runoff turbulence, and decreased the soil infiltration, and finally resulted in the *RD* increased (Wen et al. 2012). Similarly, the *RA* also substantially affected the runoff amount; it was the water source of runoff generation and runoff amount. An increase in *RA* accelerated the time of runoff, increasing the *RD* (Zhan et al. 1998). Besides, the *D*, *RA*, *R*, and I_{30} were the dominant contributors to the *RD* for rainfall pattern A. The *R*, I_{30}, *RA*, and *D* were the primary factors affecting the *RD* for rainfall pattern B. For rainfall pattern C, the *R*, *RA*, *I*, and I_{30} substantially influenced the *RD*. This result indicated that these rainfall parameters were the dominant factors affecting the *RD*. The *D* affected soil infiltration, an increase in *D* promotes more rainfall become to runoff (Bai et al. 2024). The higher the I_{30}, the higher the *I*, the increase in these values might exceed the soil infiltration capacity, resulting in insufficient time for rainfall to infiltrate, triggering surface runoff (Zheng et al. 2016; Sobol et al. 2017).

In addition, surface runoff generated by rainfall is the carrier of the occurrence of water erosion (Frauenfeld & Truman 2004). The *RD*, *R*, and *RA* were the main factors affecting sediment transport for all rainfall patterns. The *RD* contributed the most to the *SY*, because it reflects the synergistic interaction between rainfall and the surface, serving as the fundamental driving force for sediment generation and determining the sediment transport capacity (Dai et al. 2022). As the *RD* increased, the interaction effect of raindrop impact and runoff scouring increased; more water was available to transport sediments, and the sediment carrying capacity increased (Ding et al. 2024). Besides, the *R* and *RA* directly and indirectly affected the *SY* by influencing the *RD*. As the *R* increased, more loose soil particles were generated, and the soil detachment capacity and sediment transport capacity increased (Wen et al. 2012). An increase in *RA* resulted in an increased runoff amount and then sediment carrying capacity, and more soil particles were transported (Sobol et al. 2017). Furthermore, the I_{30}, *RA*, and *S* contributed the most to the *SY* for rainfall pattern A. The *R*, *D*, *VC*, and *RD* were crucial factors impacting the *SY* for rainfall pattern B. The *R*, *RD*, and *S* significantly affected the *SY* for rainfall pattern C. The result indicated that these rainfall parameters were the main factors affecting the *SY*, followed by the *S* and *VC*. As mentioned above, the *R* and *RD* were the key factors contributing to the *SY*. The higher the I_{30}, the higher the *I*, the raindrop impact destroyed the soil structure, resulting in more loose soil particles (Flanagan et al. 1988; Zhang et al. 2020b); an increase in runoff turbulence enhanced the sediment transport capacity (Jia et al. 2022). The soil cohesive force decreased with an increase in *S* due to the gravity effect (Nord & Esteves 2010; Wu et al. 2018). An increase in the raindrop lateral shear force reduced the soil corrosion resistance (Shen et al. 2021; Dai et al. 2022); thus, more soil particles were transported (Zheng et al. 2016; Hofbauer et al. 2023). Different results were observed in other regions due to differences in the climate, topography, and soil type, etc (Defersha et al. 2011; Balacco 2013). The *VC* reflects the vegetative, reproductive, and mature growth stages and had important impact on the *SY* (Wei et al. 2023). Dense vegetation structure reduces the raindrop impact (Wang et al. 2024). A dense root system holds the soil in place and increases the erosion resistance, decreasing the *SY* (Londero et al. 2021). The differences in *VC* between the initial and final stages of the two crops are attributed

https://doi.org/10.17221/39/2025-SWR

to their growth characteristics during the seedling, senescence, and abscission stages (Yan et al. 2023). Our results show that runoff had a significant effect on sediment transport.

CONCLUSION

The erosive rainfall events were dominated by rainfall pattern with short duration, high intensity, and low amount (50.0%). The runoff depth and sediment yield significantly increased with the slope gradients for the same rainfall pattern. Rainfall pattern C, with long duration, low rainfall intensity, and high rainfall amount, had the largest influence on the cumulative runoff depth (67.2% to 74.0%) and sediment yield (73.4% to 73.8%), it was the most destructive to soil erosion in the observation period. The rainfall erosivity and amount significantly affected the runoff depth for all rainfall patterns. The runoff depth, rainfall erosivity, and rainfall amount were key factors affecting the sediment yield.

REFERENCES

Bai Q., Zhou L.L., Fan H.M., Huang D.H., Yang D.F., Liu H. (2024): Effects of frozen layer on composite erosion of snowmelt and rainfall in the typical black soil of northeast china. Water, 16: 2131.

Balacco G. (2013): The interrill erosion for a sandy loam soil. International Journal of Sediment Research, 28: 329–337.

Chaplot V.A.M., Le Bissonnais Y. (2003): Runoff features for interrill erosion at different rainfall intensities, slope lengths, and gradients in an agricultural loessial hillslope. Soil Science Society of America Journal, 67: 844–851.

Dai T.Y., Wang L.Q., Li T.A., Qiu P.P., Wang J. (2022): Study on the characteristics of soil erosion in the black soil area of northeast China under natural rainfall conditions: The case of Sunjiagou small watershed. Sustainability, 14: 8284.

Defersha M.B., Quraishi S., Melesse A. (2011): The effect of slope steepness and antecedent moisture content on interrill erosion, runoff and sediment size distribution in the highlands of Ethiopia. Hydrology and Earth System Sciences, 15: 2367–2375.

Ding G.H., Ren Z.Z., Hu W., Chen Y., Zhang X.Y. (2024): Effects of erosive rainfall on soil erosion characteristics of black sloping farmland. Journal of Soil and Water Conservation, 38: 47–56.

Flanagan D.C., Foster G.R., Moldenhauer W.C. (1988): Storm pattern effect on infiltration, runoff, and erosion. Transactions of the American Society of Agricultural and Biological Engineers, 31: 414–420.

Frauenfeld B., Truman C. (2004): Variable rainfall intensity effects on runoff and interrill erosion from two coastal plain ultisols in Georgia. Soil Science, 169: 143–154.

Hofbauer M., Kincl D., Vopravil J., Kabelka D., Vrablik P. (2023): Preferential erosion of soil organic carbon and fine-grained soil particles-an analysis of 82 rainfall simulations. Agronomy, 13: 217.

Jia L., Yu K.X., Li Z.B., Li P., Zhang J.Z., Wang A.N., Ma L., Xu G.C., Zhang X. (2022): Temporal and spatial variation of rainfall erosivity in the loess plateau of China and its impact on sediment load. Catena, 210: 105931.

Juliev M., Kholmurodova M., Abdikairov B., Abuduwaili J. (2024): A comprehensive review of soil erosion research in central asian countries (1993–2022) based on the Scopus database. Soil and Water Research, 19: 244–256.

Liu B.Y., Zhang G.L., Xie Y., Shen B., Gu Z.J., Ding Y.Y. (2021): Delineating the black soil region and typical black soil region of northeastern China. Chinese Science Bulletin, 66: 96–106.

Londero A.L., Minella J.P.G., Schneider F.J.A., Deuschle D., Merten G.H., Evrard O., Boeni M. (2021): Quantifying the impact of no-till on sediment yield in southern Brazil at the hillslope and catchment scales. Hydrological Processes, 35: e14286.

Meng X.M., Zhu Y., Yin M.S., Liu D.F. (2021): The impact of land use and rainfall patterns on the soil loss of the hillslope. Scientific Reports, 11: 16341.

Neves dos Santos J.C., de Andrade E.M., Augusto Medeiros P.H., Simas Guerreiro M.J., de Queiroz Palacio H.A. (2017): Land use impact on soil erosion at different scales in the Brazilian semi-arid. Revista Ciencia Agronomica, 48: 251–260.

Nishigaki T., Sugihara S., Kilasara M., Funakawa S. (2017): Surface runoff generation and soil loss under different soil and rainfall properties in the Uluguru Mountains, Tanzania. Land Degradation & Development, 28: 283–293.

Nord G., Esteves M. (2010): The effect of soil type, meteorological forcing and slope gradient on the simulation of internal erosion processes at the local scale. Hydrological Processes, 24: 1766–1780.

Parsons A.J., Stone P.M. (2006): Effects of intra-storm variations in rainfall intensity on interrill runoff and erosion. Catena, 67: 68–78.

Pena-Angulo D., Nadal-Romero E., Gonzalez-Hidalgo J.C., Albaladejo J., Andreu V., Bahri H., Bernal S., Biddoccu M., Bienes R., Campo J., Campo-Bescos M.A., Canatario-Duarte A., Canton Y., Casali J., Castillo V., Cavallo E., Cerda A., Cid P., Cortesi N., Desir G., Diaz-Pereira E., Espigares T., Estrany J., Farguell J., Fernandez-Raga M., Ferreira C.S., Ferro V., Gallart E., Gimenez R., Gimeno E., Gomez J.A., Gomez-Gutierrez A., Gomez-

https://doi.org/10.17221/39/2025-SWR

Macpherson H., Gonzalez-Pelayo O., Kairis O., Karatzas G.P., Keesstra S., Klotz S., Kosmas C., Lana-Renault N., Lasanta T., Latron J., Lazaro R., Le Bissonnais Y., Le Bouteiller C., Licciardello F., Lopez-Tarazon A., Lucia A., Marin-Moreno V.M., Marin C., Marques M.J., Martinez-Fernandez J., Martinez-Mena M., Mateos L., Mathys N., Merino-Martin L., Moreno-de las Heras M., Moustakas N., Nicolau J.M., Pampalone V., Raclot D., Rodriguez-Blanco M.L., Rodrigo-Comino J., Romero-Diaz A., Ruiz-Sinoga J.D., Rubio J.L., Schnabel S., Senciales-Gonzalez J.M., Sole-Benet A., Taguas E.V., Taboada-Castro M.T., Taboada-Castro M.M., Todisco E., Ubeda X., Varouchakis E.A., Wittenberg L., Zabaleta A., Zorn M. (2020): Relationship of weather types on the seasonal and spatial variability of rainfall, runoff, and sediment yield in the western mediterranean basin. Atmosphere, 11: 609.

Peng T., Wang S.J. (2012): Effects of land use, land cover and rainfall regimes on the surface runoff and soil loss on karst slopes in southwest China. Catena, 90: 53–62.

Qin W., Zuo C.Q., Yan Q.H., Wang Z.Y., Du P.F., Yan N. (2015): Regularity of individual rainfall soil erosion in bare slope land of red soil. Transactions of the Chinese Society of Agricultural Engineering, 31: 124–132.

Shen H.O., Ma R.M., Ye Q., Feng J., Wang J.H. (2021): Impacts of corn straw coverage and slope gradient on soil erosion and sediment size distributions in the Mollisol region, NE China. Eurasian Soil Science, 54: 2000–2008.

Sobol N.V., Gabbasova I.M., Komissarov M.A. (2017): Effect of rainfall intensity and slope steepness on the development of soil erosion in the southern cis-ural region (a model experiment). Eurasian Soil Science, 50: 1098–1104.

Sun T., Cruse R.M., Chen Q., Li H., Song C.Y., Zhang X.Y. (2014): Design and initial evaluation of a portable in situ runoff and sediment monitoring device. Journal of Hydrology, 519: 1141–1148.

Tao W.H., Wu J.H., Wang Q.J. (2017): Mathematical model of sediment and solute transport along slope land in different rainfall pattern conditions. Scientific Reports, 7: 44082.

Wang F., Tian P., Guo W.Z., Chen L., Gong Y.W., Ping Y.D. (2024): Effects of rainfall patterns, vegetation cover types and antecedent soil moisture on run-off and soil loss of typical luvisol in southern China. Earth Surface Processes and Landforms, 49: 2998–3012.

Wang R.H., Wang N., Fan Y.C., Sun H., Fu H.P., Yang J.C. (2022): Quantitative attribution analysis of the spatial differentiation of gully erosion in the black soil region of northeast China. Geofluids, 2022: 1652.

Wei B., Li Z.W., Duan L.X., Gu Z.K., Liu X.M. (2023): Vegetation types and rainfall regimes impact on surface runoff and soil erosion over 10 years in karst hillslopes. Catena, 232: 107443.

Wei W., Chen L.D., Fu B.J., Huang Z.L., Wu D.P., Gui L.D. (2007): The effect of land uses and rainfall regimes on runoff and soil erosion in the semi-arid loess hilly area, China. Journal of Hydrology, 335: 247–258.

Wen L.L., Zheng F.L., Yang Q.S., Shen H.O. (2012): Effects of rainfall patterns on hillslope farmland erosion in black soil region of northeast China. Journal of Hydraulic Engineering, 43: 1084–1091.

Wu L.L., Wang Y.Q., Wang C.F., Wang Y.J., Wang B. (2017): Effect of rainfall patterns on hillslope soil erosion in rocky mountain area of north China. Transactions of the Chinese Society of Agricultural Engineering, 33: 157–164.

Wu L., Peng M.L., Qiao S.S., Ma X.Y. (2018): Effects of rainfall intensity and slope gradient on runoff and sediment yield characteristics of bare loess soil. Environmental Science and Pollution Research, 25: 3480–3487.

Yan Y., Jiang Y.Y., Guo M.M., Zhang X.Y., Chen Y., Xu J.Z. (2023): Effects of grain-forage crop type and natural rainfall regime on sloped runoff and soil erosion in the Mollisols region of Northeast China. Catena, 222: 106888.

Yang P.P., Li R., Gu Z.K., Qin L., Song T., Liu Z.X., Gao J.Y., Yuan J. (2022): Runoff sediment characteristics affected by erosive rainfall patterns in a small watershed in karst areas of southwest China. Catena, 219: 106591.

Yao X.L., Yu J.S., Jiang H., Sun W.C., Li Z.J. (2016): Roles of soil erodibility, rainfall erosivity and land use in affecting soil erosion at the basin scale. Agricultural Water Management, 174: 82–92.

Zhan M., Li Z.C., Xin Y.L. (1998): On the relationship between precipitation parameter and soil erosion. Journal of Heilongjiang Hydraulic Engineering College, 1: 40–43.

Zhang X., Cao L., Du J., Wang Y.D., Han J.L. (2020a): Comprehensive observation of precipitation changes in the three provinces of Northeast China from 1961–1990 and 1991–2018. Jiangsu Agricultural Sciences, 48: 282–287.

Zhang X.Y., Qiao B.L., Li J.Y., Qi Z., Yan Y., Zhen H.C., Hu W. (2020b): Effects of rainfall intensity and slope on splash erosion characteristics of downslope ridge on farmland in black soil areas of northeast china. Transactions of the Chinese Society of Agricultural Engineering, 36: 110–117.

Zheng F.L., Bian F., Lu J., Qin C., Xu X.M. (2016): Effects of rainfall patterns on hillslope erosion with longitudinal ridge in typical black soil region of northeast china. Transactions of the Chinese Society for Agricultural Machinery, 47: 90–97.

Received: April 1, 2025
Accepted: September 17, 2025
Published online: January 4, 2026